Bone 130 (2020) 115062

Contents lists available at ScienceDirect

Bone

journal homepage: www.elsevier.com/locate/bone

Full length article

Mice lacking plastin-3 display a specific defect of cortical bone acquisition

Timur Alexander Yorgan[a,1], Hatice Sari[a,1], Tim Rolvien[a], Sabine Windhorst[b], Antonio Virgilio Failla[c], Uwe Kornak[d,e], Ralf Oheim[a], Michael Amling[a], Thorsten Schinke[a,*]

[a] Department of Osteology and Biomechanics, University Medical Center Hamburg-Eppendorf, 20246 Hamburg, Germany
[b] Department of Biochemistry and Signal Transduction, University Medical Center Hamburg-Eppendorf, 20246 Hamburg, Germany
[c] Microscopy Core Facility, University Medical Centre Hamburg-Eppendorf, 20246 Hamburg, Germany
[d] Institute of Medical Genetics and Human Genetics, Charité-Universitätsmedizin Berlin, 13353 Berlin, Germany
[e] Berlin Brandenburg Center for Regenerative Therapies (BCRT), Charité-Universitätsmedizin Berlin, 13353 Berlin, Germany

ARTICLE INFO

Keywords:
Bone remodeling
Cortical bone
Plastin-3
X-linked osteoporosis

ABSTRACT

Although inactivating mutations of *PLS3*, encoding the actin-bundling protein plastin-3, have been identified to cause X-linked osteoporosis, the cellular and molecular influence of PLS3 on bone remodeling is poorly defined. Moreover, although a previous study has demonstrated moderate osteopenia in 12 week-old *Pls3*-deficient mice based on μCT scanning, there is no reported analysis of such a model on the basis of undecalcified histology and bone-specific histomorphometry. To fill this knowledge gap we applied a deep phenotyping approach and studied *Pls3*-deficient mice at different ages. Surprisingly, we did not detect significant differences between wildtype and *Pls3*-deficient littermates with respect to trabecular bone mass, and the same was the case for all histomorphometric parameters determined at 12 weeks of age. Remarkably however, the cortical thickness in both, tibia and femur, was significantly reduced in *Pls3*-deficient mice in all age groups. We additionally studied the *ex vivo* behavior of *Pls3*-deficient primary osteoblasts, which displayed moderately impaired mineralization capacity. Of note, while most osteoblastogenesis markers were not differentially expressed between wildtype and *Pls3*-deficient cultures, the expression of *Sfrp4* was significantly reduced in the latter, a potentially relevant finding, since Sfrp4 inactivation, in mice and humans, specifically causes cortical thinning. We finally addressed the question, if *Pls3*-deficiency would impair the osteoanabolic influence of parathyroid hormone (PTH). For this purpose we applied daily injection of PTH into wildtype and *Pls3*-deficient mice and found a similar response regardless of the genotype. Taken together, our data reveal that *Pls3*-deficiency in mice only recapitulates the cortical bone phenotype of individuals with X-linked osteoporosis by negatively affecting the early stage of cortical bone acquisition.

1. Introduction

Plastin-3 (PLS3, also known as T-plastin) is one member, together with Pls1 and Pls2, of a protein family binding to individual actin filaments to promote their assembly into actin bundles [1]. Since the actin cytoskeleton is of central importance for many cellular processes, and since *Pls3* is expressed in various tissues, it is surprising that mutational inactivation of human *PLS3* specifically affects the skeleton [2–8]. In fact, mutations of the *PLS3* gene, which is located on the X-chromosome, were identified to segregate with X-linked osteoporosis in different families [2–4]. Moreover, a rare *PLS3* variant was found to be associated with increased fracture risk in female heterozygous carriers [2,6]. The analysis of patients displaying *PLS3*-dependent X-linked osteoporosis further revealed that the disease manifests in early childhood and affects both, trabecular and cortical bone mass [3]. Moreover, evaluation of transiliac bone biopsies from affected patients revealed that there are specific defects of bone matrix mineralization, which may be linked to inactivation of PLS3 function [3,4,7]. Until now, most of the respective patients are treated by bisphosphonate administration, yet a pilot study involving three patients with *PLS3* splice site mutations has suggested, that they respond normally to teriparatide injection [9].

Despite the overwhelming genetic evidence supporting a key function of PLS3 in bone mass acquisition, the influence of PLS3 on skeletal cell types is poorly understood at the cellular and molecular level. It

* Corresponding author at: Department of Osteology and Biomechanics, University Medical Center Hamburg Eppendorf, Martinistrasse 52, Hamburg 20246, Germany.
E-mail address: schinke@uke.de (T. Schinke).
[1] These authors contributed equally to this work.

https://doi.org/10.1016/j.bone.2019.115062
Received 5 June 2019; Received in revised form 9 September 2019; Accepted 10 September 2019
Available online 31 October 2019

was suggested, based on osteocyte expression of the chicken homologue of PLS3, that the protein function may be linked to mechanosensing by osteocytes [10]. An alternative explanation for the impact of PLS3 on bone mass was recently established based on a first analysis of *Pls3*-deficient mice. Here it was found that these mice, at 12 weeks of age, display moderate osteopenia, potentially explained by increased osteoclast activity [11]. A moderate, yet opposite phenotype was observed in a mouse model with ubiquitous *Pls3* over-expression, and here osteoclast function was impaired due to inhibition of NFκB signaling and *Nfatc1* transcription [11]. Whether this influence on osteoclastogenesis is the only function of PLS3 in bone remodeling regulation remains to be established, since there is still no reported analysis of *Pls3*-deficient mice on the basis of undecalcified histology and histomorphometry.

Here we report such an analysis, where we compared *Pls3*-deficient mice towards wildtype littermate controls at four different ages. Unexpectedly, we did not observe any impact of *Pls3*-deficiency on trabecular bone parameters. Importantly however, cortical bone mass was significantly decreased in all age groups, thereby demonstrating a critical function of PLS3 in the early stages of cortical bone mass acquisition. We finally demonstrate that *Pls3*-deficient mice respond normally to daily injection of PTH, thereby confirming that the respective patients might profit from teriparatide treatment.

2. Materials and methods

2.1. Generation of Pls3-deficient mice and animal husbandry

Mice were revitalized from commercially available embryos harboring a *Pls3* KO-First construct (C57BL/6N-A^{tm1Brd} *Pls3*$^{tm1a(EUCOMM)Wtsi}$/WtsiOulu, EMMA). Genotyping was performed using primers (5′-TAC GCC ATT ACT CCC CAT CC-3′, 5′-TTT CAC ACA CTC GCC AAA CAC-3′ and 5′-TCG TGG TAT CGT TAT GCG CC-3′) detecting a 581-bp wildtype or 311-bp *Pls3*-KO allele. All mice were kept in a specific pathogen-free environment with a 12 -h light/dark cycle, 45–65 % relative humidity and 20–24 °C ambient temperature in open or individually ventilated cages with wood shavings bedding and nesting material in groups not surpassing 6 animals. The mice had access to tap water and standard rodent chow (1328 P, Altromin Spezialfutter GmbH & Co. KG, Germany) *ad libitum*.

2.2. Treatment of Pls3-deficient mice

Mice were treated for 2 weeks by daily intraperitoneal injection of 80 μg/kg recombinant human PTH 1-34. Littermate mice were allocated randomly to treatment groups and endpoint measurements (μCT and histomorphometry) were performed in a blinded fashion. After initiation of treatment the welfare of the mice was assessed daily based on overall appearance and body weight. No unexpected or severe adverse events were observed. All animal experiments were approved by the animal facility of the University Medical Center Hamburg-Eppendorf and by the "Behörde für Soziales, Familie, Gesundheit und Verbraucherschutz" (G117/16, G034/17 and Org869).

2.3. Histology

To allow quantification of the bone formation rate, all animals received two doses of calcein (30 mg/kg i.p., Sigma–Aldrich Corp., USA) 10 and 3 days before sacrifice. The skeletons were fixed in 3.7% PBS-buffered formaldehyde over night and subsequently stored in 80% ethanol. The lumbar vertebral bodies L1 to L4 and the left tibia of each mouse were embedded in methylmetacrylate as previously described [12]. Histological sections of 4 μm thickness from the sagittal plane were stained by toluidine blue and von Kossa/van Gieson staining procedures as described [13]. Histomorphometry was performed according to the ASBMR guidelines [14] using the OsteoMeasure histomorphometry system (Osteometrics Inc., USA). Kinetic parameters of the cortical bone were assessed on transverse sections.

2.4. Bone mineral density distribution

For analysis of bone mineral density distribution, a quantitative backscattered electron imaging (qBEI) was performed on embedded tibiae coated with carbon. Identical regions of interest in the cortical tibiae were analyzed using a scanning electron microscope (LEO 435 VP; LEO Electron Microscopy Ltd., Cambridge, UK) operated at 20 kV and 680pA using constant working distance of 20 mm (BSE Detector, Type 202; K.E. Developments Ltd., Cambridge, UK). For analysis, grey-value images were utilized according to previously described protocols [15–17]. The system was calibrated using a carbon-aluminium standard, facilitating the quantification of bone mineral as calcium weight percentage.

2.5. μCT analysis

For μCT analysis the right femur of each mouse extracted from the fixed skeletons. μCT scanning and analysis was performed with a voxel resolution of 10 μm as previously described using a μCT 40 desktop cone-beam microCT (Scanco Medical, Switzerland) [18] according to standard guidelines [19]. Trabecular bone was analyzed in the distal metaphysis in a volume situated 2500 μm to 500 μm proximal of the distal growth plate. Cortical bone was analyzed in a 1000 μm long volume situated in the middle of the diaphysis. Cortical bone evaluation was performed with a threshold value of 300 and for trabecular bone a threshold value of 250 was implemented.

2.6. Mechanical testing

Explanted femora were used for destructive three point bending tests utilizing a BZ2.5 materials testing machine and the testXpert software (both Zwick Roell) as described previously [20]. In brief, the femora were placed on support bars with 7 mm spacing and a tip was lowered medially with a constant speed of 2 mm/min until failure. The distance and force were recorded at 100 Hz and all presented parameters were internally calculated from this data by the software.

2.7. Cell culture

Bone marrow cells were isolated from the tibiae, femora and pelvis of *Pls3*$^{d/0}$ and *Pls3*$^{+/0}$ littermates. Cells were plated at a density of 5×10^6 cells/ml in α-MEM medium (Sigma-Aldrich Corp., USA) supplemented with 10% (v/v) FCS (Thermo Fisher Scientific Inc., USA) and 100 U/ml penicillin/streptomycin (Life Technologies, USA). Calvarial osteoblasts were obtained from 3-5-days old mice. Cells were isolated by sequential digestion with collagenase/dispase and plated in the same medium as mentioned above. Osteoblastogenic differentiation was induced when the cells reached 70% confluency by the addition of 50 μg/ml ascorbic acid (Sigma-Aldrich Corp., USA) and 10 mM ß-glycerophosphate (Sigma-Aldrich Corp., USA). Alizarin red staining and quantification was performed as previously described [21].

2.8. Western blotting

Proteins were isolated from cell cultures in RIPA buffer containing protease inhibitors. Equal volumes of lysate were electrophoretically separated in 12% Bolt Bis-Tris Plus gels (Thermo Fisher Scientific Inc., USA) under reducing conditions. Proteins were subsequently wet transferred to 0.2 μm nitrocellulose membranes (Bio-Rad Laboratories, Inc., USA) and blocked for 1 h in 5% BSA in TBST buffer. Primary antibody binding was performed over night at 4 °C in 5% BSA in TBST at dilutions of 1:500 (anti-Pls1, ab94605, Abcam, UK), 1:5000 (anti-Pls2, GTX105789, GeneTex, Inc., USA), 1:500 (anti-Pls3, SAB2700266,

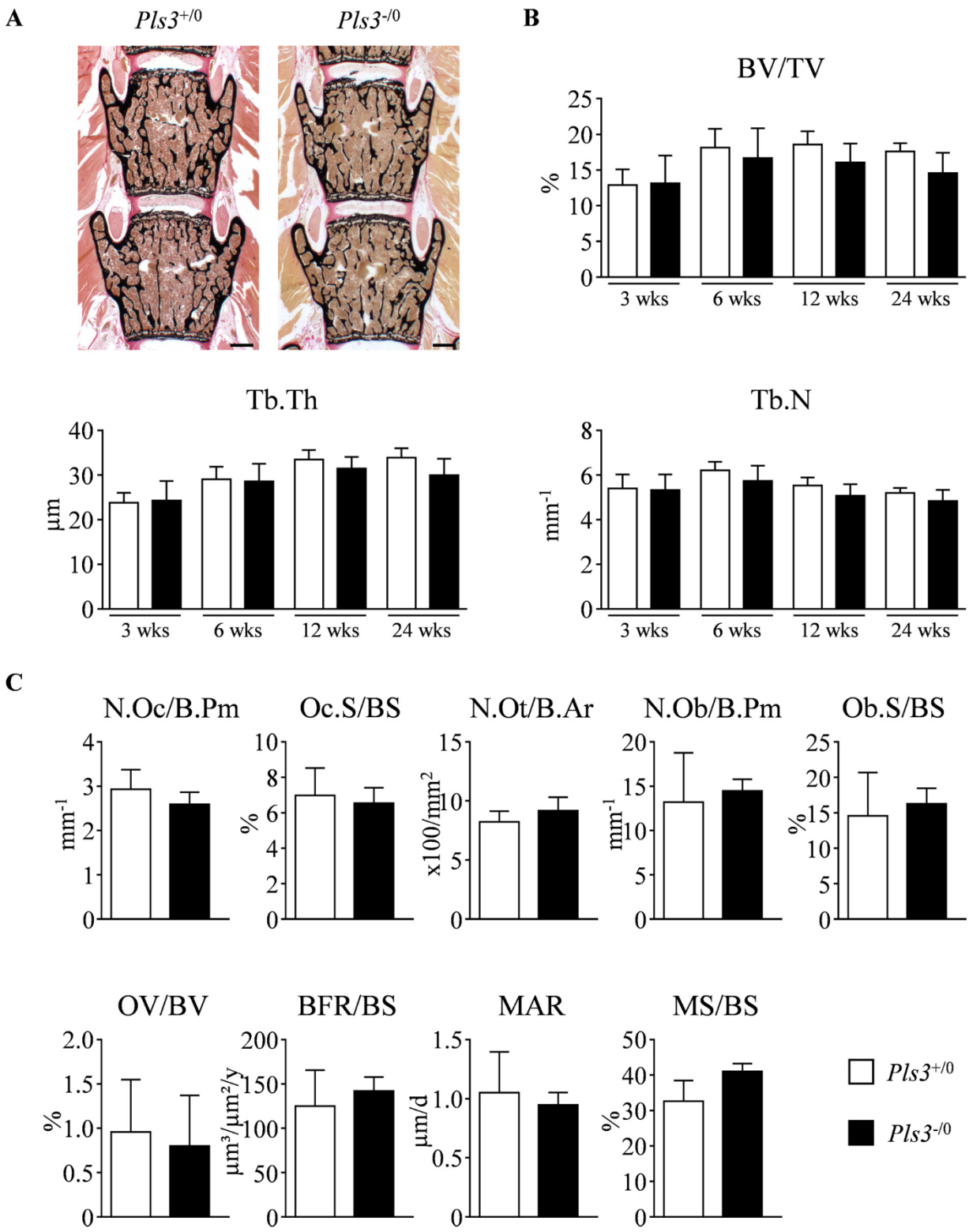

Fig. 1. Undecalcified histology of vertebral bodies from *Pls3*-deficient mice. (A) Representative undecalcified histological sections of vertebral bodies L3 and L4 from 12 weeks old, male *Pls3*$^{+/0}$ and *Pls3*$^{-/0}$ mice. Scale bar = 500 µm. (B) Structural histomorphometric parameters of the vertebral trabecular bone of male *Pls3*$^{+/0}$ and *Pls3*$^{-/0}$ mice at the indicated ages. (C) Cellular and dynamic histomorphometric parameters of 12 week old male *Pls3*$^{+/0}$ and *Pls3*$^{-/0}$ mice. Data were analyzed by Student's *t*-test. n ≥ 5 mice per group. *p < 0.05 vs. controls.

Sigma-Aldrich Corp., USA) and 1:1000 (anti-α-Tubulin, #2125, Cell Signaling Technology Corp., UK), followed by incubation for 1 h with an HRP-conjugated secondary antibody against rabbit IgG (1:2000 diluted in 5% BSA in TBST buffer, Dako P0448, Agilent Technologies, Inc., USA). Signals were detected using Pierce™ ECL Western Blotting Substrate (Thermo Fisher Scientific Inc., USA) in a digital gel documentation imaging system (Bio-Rad Laboratories, Inc., USA) with exposure times of 5–10 min. Quantification of specific signals was performed with the Quantity One software (Bio-Rad Laboratories, Inc., USA).

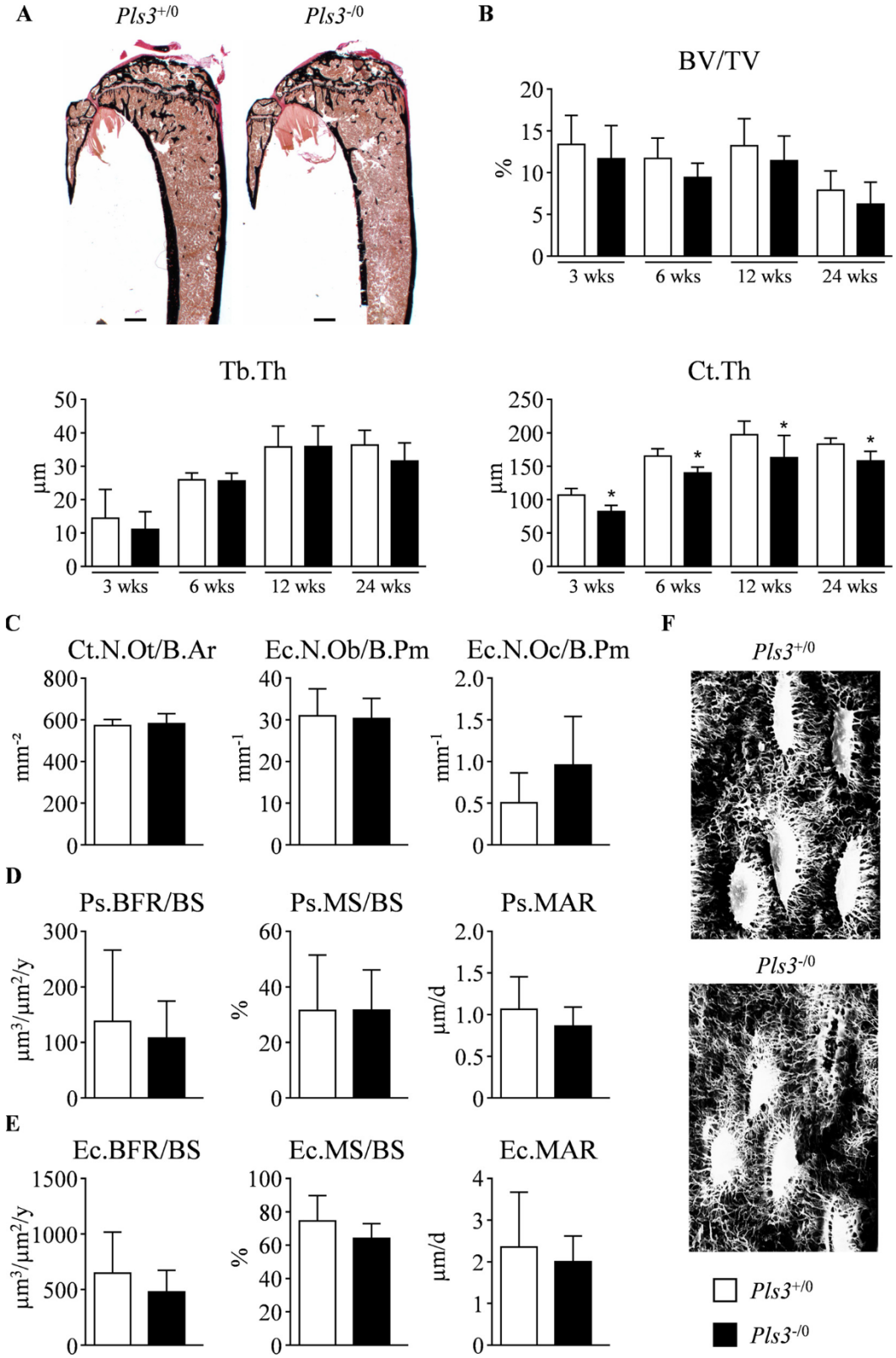

Fig. 2. Undecalcified histology of tibiae from *Pls3*-deficient mice. (A) Representative undecalcified histological sections of tibiae from 12 weeks old, male $Pls3^{+/0}$ and $Pls3^{-/0}$ mice. Scale bar = 500 µm. (B) Structural histomorphometric parameters of the tibiae of male $Pls3^{+/0}$ and $Pls3^{-/0}$ mice at the indicated ages. (C) Cellular histomorphometric parameters determined in the tibial cortical bone or on the endocortical surface of 12 weeks old male $Pls3^{+/0}$ and $Pls3^{-/0}$ mice. (D) Dynamic histomorphometric parameters of 12 weeks old male $Pls3^{+/0}$ and $Pls3^{-/0}$ mice determined on the periosteal surface. (E) Dynamic histomorphometric parameters of 12 weeks old male $Pls3^{+/0}$ and $Pls3^{-/0}$ mice determined on the endocortical surface. (F) Representative scanning electron micrographs of cortical osteocytes in the tibia of 12 weeks old male $Pls3^{+/0}$ and $Pls3^{-/0}$ mice. Data were analyzed by Student's *t*-test. n ≥ 5 mice per group. *p < 0.05 vs. controls.

2.9. Expression analysis

RNA was isolated using the Nucleospin RNA II kit (Macherey-Nagel GmbH & Co. KG, DE). Concentration and quality of RNA were measured using a NanoDrop ND-1000 system (Thermo Fisher Scientific Inc., USA) and the TapeStation 2200 instrument (Agilent Technologies Inc., USA). For qRT-PCR expression analysis RNA was reversed transcribed using Verso cDNA Synthesis Kit (Thermo Fisher Scientific Inc., USA) according to manufacturer's instructions. The quantitative expression analysis was performed using a StepOnePlus system and predesigned TaqMan gene expression assays (*Pls1,* Mm01223669_m1; *Pls2/Lcp1*, Mm01310735_m1; *Pls3*, Mm00521302_m1; *Runx2*, Mm00501580_m1; *Sp7*, Mm00504574_m1; *Alpl*, Mm00475834_m1; *Bglap*, Mm03413826_mH; *Col1a1*, Mm00801666_g1; *Ibsp*, Mm00492555_m1; *Dmp1*, Mm01208363_m1; *Postn*, Mm00450111_m1; *Sfrp4*, Mm00840104_m1; *Sharpin*, Mm00550584_m1; *Wnt16,* Mm00446420_m1, Applied Biosystems Inc., USA,). Gapdh expression was used as an internal control. Relative quantification was performed according to the $\Delta\Delta C_T$method.

2.10. Biochemical assays

Serum concentrations of biomarkers were measured by ELISA according to the manufacturer's instructions. PICP: SEA570MU (Cloud-Clone Corp., PRC); PINP: SEA957Mu (Cloud-Clone Corp., PRC); Sfrp4: MBS907810 (MyBioSource Inc., USA), two-fold dilution; Wnt16: OKCA02187 (Aviva Systems Biology, USA) two-fold dilution; CTx: AC-06F1 (Immunodiagnostic Systems Holdings PLC, UK); Rankl: E90855 KU (Wuhan USCN Business Co., Ltd, PRC), two-fold dilution; Opg: MOP00 (R&D Systems, USA), five-fold dilution.

2.11. Patient analysis

A 22 years old male patient presented in our outpatient clinic with two previous atraumatic vertebral fractures (Th7, L2). Since osteologic assessment at our department includes, for all individuals displaying early-onset osteoporosis, a genetic screen for mutations in genes associated with skeletal disorders, we identified a hemizygous intronic mutation (1512-1G > T) of *PLS3*. A diagnostic transiliac crest biopsy had been obtained from the patient at the age of 18 years. Here we performed histomorphometry and BMDD analyses in the same way as described for the mice. Published reference values, which were previously validated in our own cohort, were used for comparison [22–25]. All patient data were obtained during standard clinical care according to the World Medical Association Declaration of Helsinki. Written informed consent was obtained from the patient. Dual energy X-ray absorptiometry (DXA, Lunar iDXA, GE Healthcare; Madison, WI, USA) and high-resolution peripheral quantitative computed tomography (HR-pQCT, XtremeCT, Scanco Medical, Switzerland) scans were performed according to standard clinical procedures. Serum parameters were determined in the Department of Clinical Chemistry, University Medical Center Hamburg-Eppendorf according to standard procedures and were compared with the age- and gender-matched reference range.

2.12. Statistical analysis

All data presented in the manuscript are presented as means ± standard deviations. Statistical analysis was performed using D'Agostino-Pearson omnibus normality test and unpaired, two-tailed Student's *t*-test with Bonferroni correction for multiple testing where applicable, using Prism (GraphPad Software Inc., USA). P-values below 0.05 were considered statistically significant. Sample size and power of analysis for animal experiments was determined by an *a priorit*-test with G*Power [26]. The exact sample size for each dataset is listed in supplementary Table 1.

2.13. Data availability

All data have been provided within the manuscript.

3. Results

We first analyzed undecalcified sections of vertebral bodies from male *Pls3*-deficient mice and wildtype littermates at the ages of 3, 6, 12 and 24 weeks (Fig. 1A). Quantification of the trabecular bone volume revealed that there was no difference between the groups at any age, and the same was the case for trabecular thickness and trabecular number (Fig. 1B). Since the previously described moderate osteopenia in *Pls3*-deficient males was observed at 12 weeks of age [11], we focused on this time point to apply cellular and dynamic histomorphometry. Consistent with the absence of a trabecular bone phenotype we did not observe any difference between wildtype and *Pls3*-deficient littermates in terms of bone cell numbers, osteoid volume or bone formation parameters (Fig. 1C).

We additionally analyzed tibia sections from the same mice (Fig. 2A). Here we also did not observe changes of trabecular bone mass in *Pls3*-deficient mice, yet the cortical thickness was significantly reduced towards wildtype controls in all age groups (Fig. 2B). To find a possible explanation for this observation we determined the number of cortical osteocytes and of endocortical osteoblasts and osteoclasts in 12 weeks old mice (Fig. 2C). We did not observe statistically significant differences between the two genotypes for any of these parameters, and the same was the case for periosteal and endosteal bone formation parameters (Fig. 2D,E). Furthermore, no morphological abnormalities were detected in *Pls3*-deficient osteocytes (Fig. 2F). Finally, we did not observe significant differences in the serum levels of bone turnover markers between 12 weeks old wildtype and Pls3-deficient mice, and the same was the case for the Rankl/Opg ratio (Fig. S1).

We additionally analyzed the femora from mice of all age groups via μCT scanning (Fig. 3A). Similar to the phenotype observed in the vertebral bodies, *Pls3*-deficiency had no major impact on the distal metaphyseal trabecular bone compartment. More specifically, the bone volume fraction was only moderately reduced in 3 weeks old *Pls3*-deficient mice, for all other age groups no significant difference was observed (Fig. 3B). Importantly however, *Pls3*-deficient mice displayed significant reduction of cortical thickness throughout all age groups (Fig. 3C and D). Nonetheless, the cortical bone gain, when related to the data of 3 weeks old mice, did not differ between wildtype and *Pls3*-deficient animals (Fig. 3E), thereby demonstrating an early establishment of the phenotype. We additionally observed moderate cortical bone porosity in 6, 12 and 24 weeks *Pls3*-deficient mice (Fig. 3F), consistent with the previously described role of PLS3 as a negative regulator of osteoclastogenesis [11]. We also performed three-point-bending assays with the femoral bones of 12 weeks old male mice. Here we detected reduced biomechanical stability caused by *Pls3*-deficiency (Fig. S2), consistent with previously published data [11]. Moreover, the analysis of 12 weeks old female mice revealed reduced cortical thickness in homozygous *Pls3*-deficient mice, and here there was also a moderate reduction of the trabecular bone mass observed (Fig. S3).

In an attempt to understand the underlying cellular pathologies caused by *Pls3*-deficiency we first monitored the expression of all *Pls* genes in different tissues and primary bone cell cultures from wildtype mice (Fig. S4). Here we identified a broad expression pattern for all of them, but also a robust, yet no differential expression of *Pls3* in primary osteoblasts. That the cortical bone phenotype of *Pls3*-deficient mice is mostly attributed to an osteoblast defect was further supported by a closer inspection of tibia sections from 3 weeks old mice (Fig. S5). Here we observed that the difference in cortical thickness between wildtype and *Pls3*-deficient mice does not originate in the bone collar region, but in the distance of 4 mm below the growth plate, where the layer of periosteal osteoblasts was disrupted in *Pls3*-deficient animals. To study the potential impact of *Pls3*-deficiency on osteoblast differentiation we

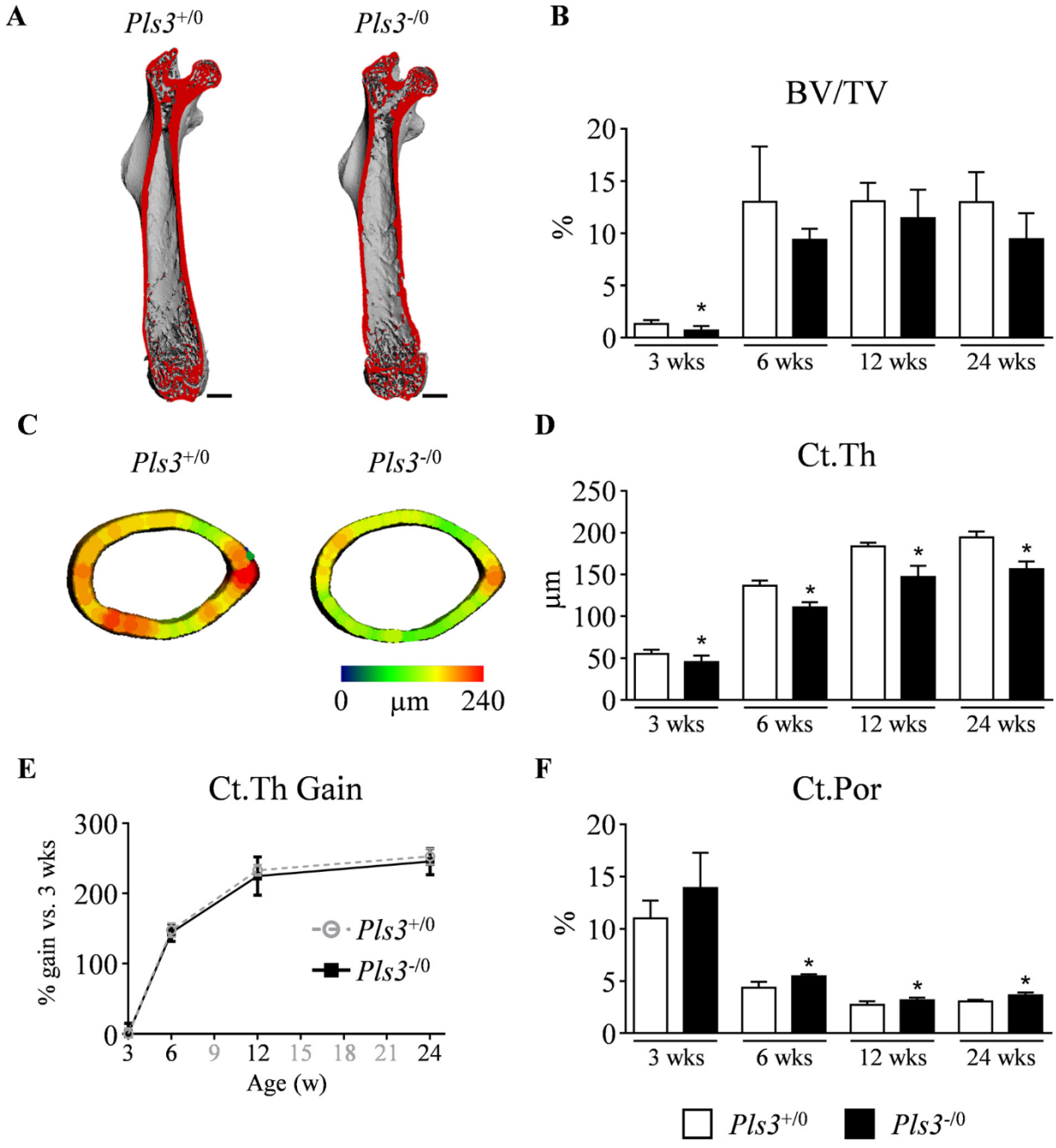

Fig. 3. µCT analysis of femora from *Pls3*-deficient mice. (A) Representative µCT images of the femora from 12 weeks old male $Pls3^{+/0}$ and $Pls3^{-/0}$ mice. The virtual cutplane appears red. Scale bar = 1 mm. (B) Trabecular bone volume in the distal femoral metaphysis of male $Pls3^{+/0}$ and $Pls3^{-/0}$ mice at the indicated ages. (C) Representative µCT images of cortical bone at the femoral mid diaphysis. The color gradient indicates the local thickness of the cortical wall. (D) Evaluation of the cortical thickness at the central femoral diaphysis of male $Pls3^{+/0}$ and $Pls3^{-/0}$ mice at the indicated ages. (E) Relative cortical thickness gain curves of $Pls3^{+/0}$ and $Pls3^{-/0}$ mice normalized to the respective cortical thickness at 3 weeks of age. (F) Cortical porosity at the central femoral diaphysis of male $Pls3^{+/0}$ and $Pls3^{-/0}$ mice at the indicated ages. Data were analyzed by Student's *t*-test. n ≥ 5 mice per group. *p < 0.05 vs. controls. (For interpretation of the references to colour in this figure legend, the reader is referred to the web version of this article.)

isolated bone marrow cells derived from wildtype and *Pls3*-deficient littermates and assessed their ability to form a mineralized matrix *ex vivo* (Fig. 4A). We thereby observed a moderate yet significant reduction in *Pls3*-deficient cultures by alizarin red staining, suggesting a cell-autonomous impairment of osteogenesis (Fig. 4B).

Similar to bone marrow cultures, *Pls3*-deficient calvarial osteoblasts also displayed moderately reduced matrix mineralization at day 15 of differentiation (Fig. 4C). At that stage we also compared wildtype and *Pls3*-deficient cultures at the level of gene expression by qRT-PCR. While *Pls3* expression was abolished in *Pls3*-deficient cells, there was no apparent compensatory induction of the other *Pls* genes (Fig. 4D). This was also confirmed by quantitative Western blotting in three independent cultures (Fig. 4E). With respect to markers of osteoblast differentiation we only observed significantly reduced expression of *Bglap*, the gene encoding osteocalcin (Fig. 4D). This led us to specifically analyze the transcription of genes with known relevance for cortical bone formation or remodeling, i.e. *Postn, Sfrp4, Sharpin* and *Wnt16* [27–32]. Here we observed reduced expression of *Sfrp4* in *Pls3*-deficient osteoblasts, which is potentially interesting, since *SFRP4* mutations cause Pyle disease, a skeletal disorder with cortical thinning as

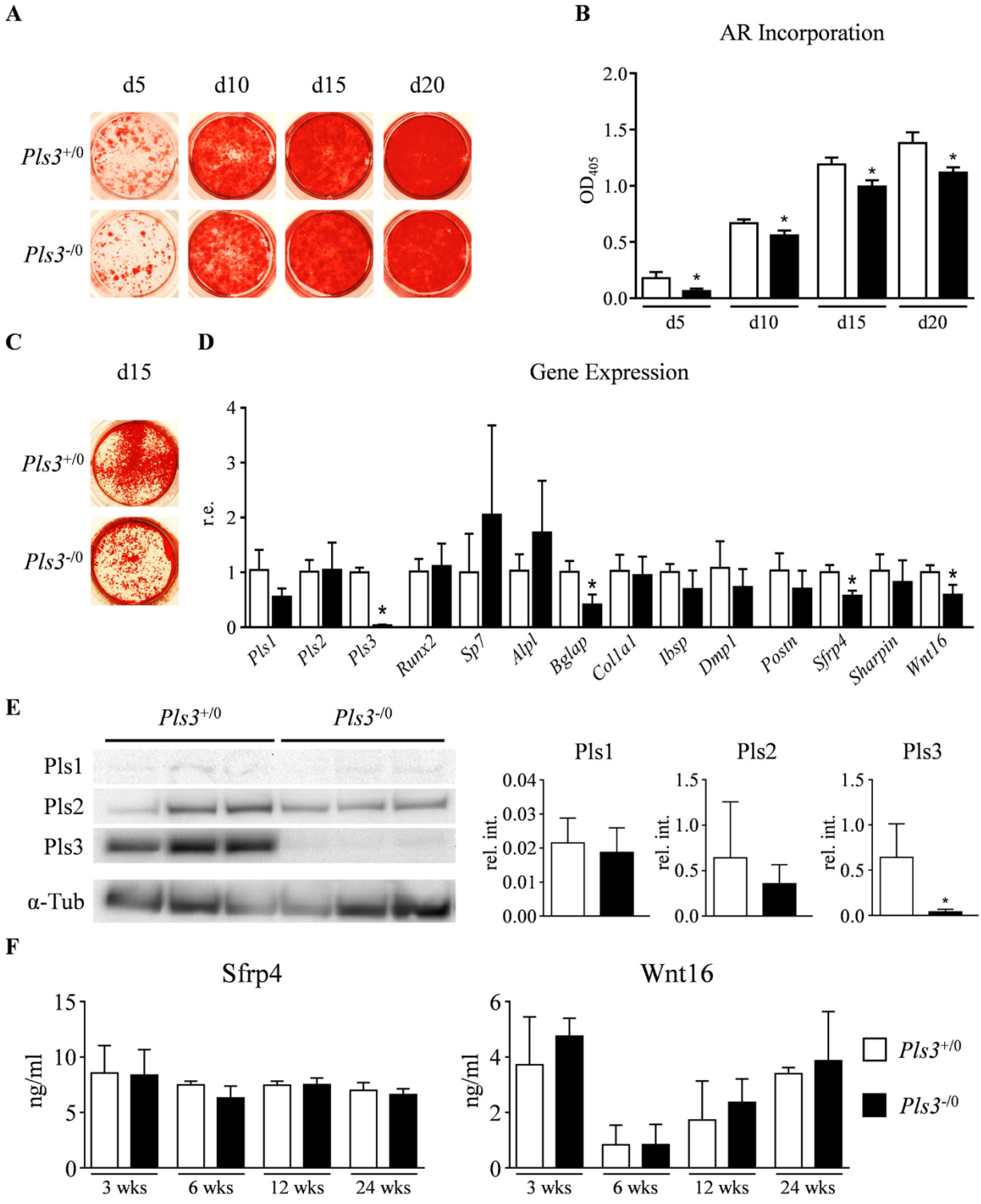

Fig. 4. Cellular phenotype of *Pls3*-deficient osteoblasts. (A) Representative images of alizarin red stained primary bone marrow cultures from $Pls3^{+/0}$ and $Pls3^{-/0}$ mice at 5 to 20 days of osteogenic differentiation as indicated. (B) Quantification of the alizarin red incorporation of primary bone marrow cultures from $Pls3^{+/0}$ and $Pls3^{-/0}$ mice at 5 to 20 days of osteogenic differentiation as indicated. n = 3 samples per group (C) Representative images of alizarin red stained primary calvarial osteoblast cultures from $Pls3^{+/0}$ and $Pls3^{-/0}$ mice at 15 days of osteogenic differentiation. (D) qRT-PCR expression analysis for the indicated genes in primary calvarial osteoblast cultures from $Pls3^{+/0}$ and $Pls3^{-/0}$ mice at 15 days of osteogenic differentiation. Shown is the relative expression compared to $Pls3^{+/0}$ cells. n = 3 samples per group. (E) Western blot for Pls proteins and α-tubulin (α-Tub) in cell lysates of primary calvarial osteoblast cultures from $Pls3^{+/0}$ and $Pls3^{-/0}$ mice at day 5 of osteogenic differentiation. Quantification of the signal intensities (normalized to α-tubulin) is given on the right. (F) Serum concentrations of Sfrp4 and Wnt16 in $Pls3^{+/0}$ and $Pls3^{-/0}$ mice at the indicated ages. n ≥ 5 mice per group. Data were analyzed by Student's *t*-test. *p < 0.05 vs. $Pls3^{+/0}$. (For interpretation of the references to colour in this figure legend, the reader is referred to the web version of this article.)

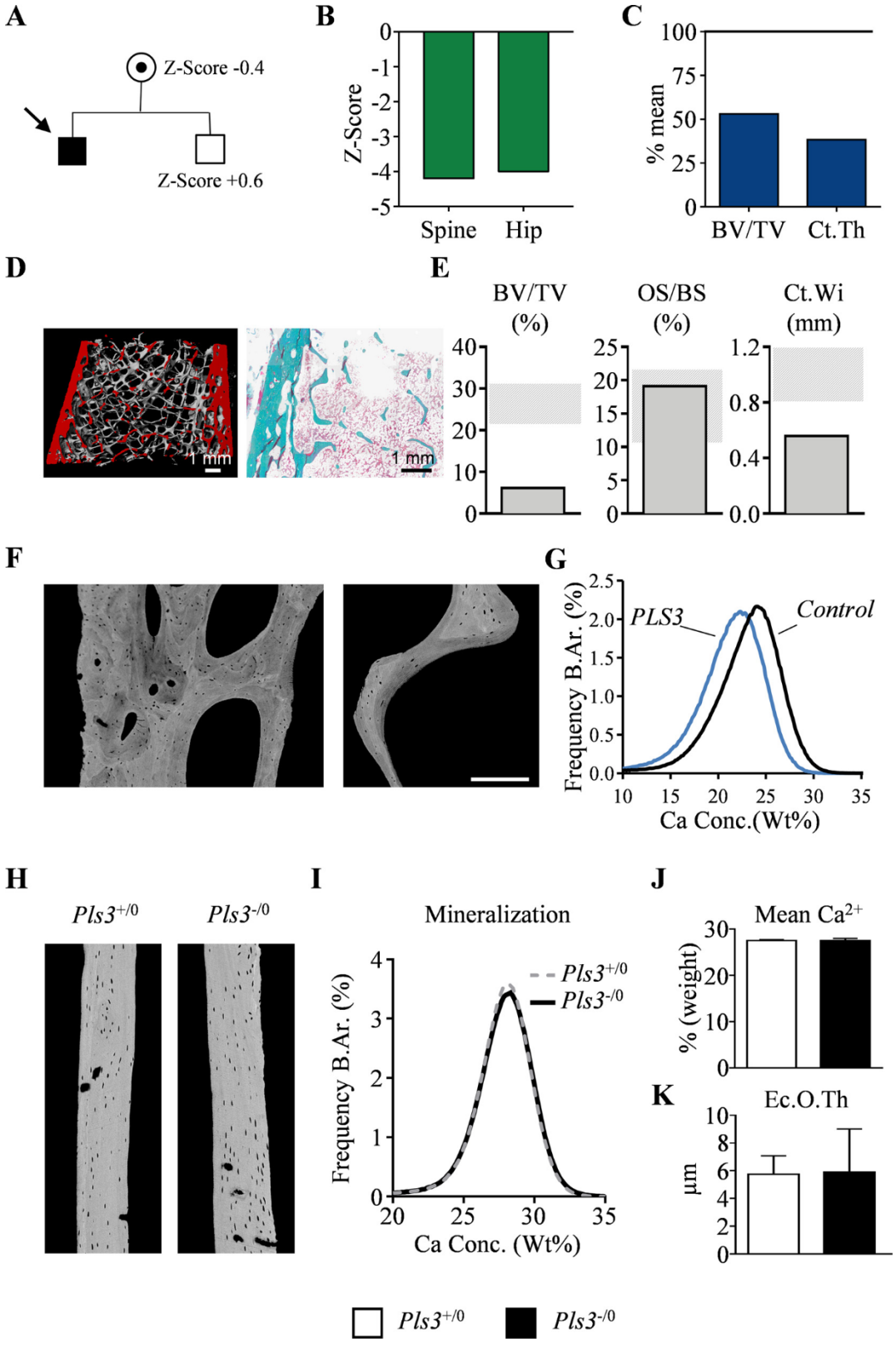

(caption on next page)

predominant feature [33–35]. We additionally found reduced expression of *Wnt16*, whose inactivation in mice is linked to cortical porosity [30]. Since Sfrp4 deficiency in mice was found to equally affect calvarial bones, we also performed µCT imaging of the skull bones from wildtype and *Pls3*-deficient mice (Fig. S6). Here we did not observe reduced calvarial thickness, yet calvarial porosity was significantly increased at 24 weeks of age. Moreover, there were no significant differences observed between wildtype and *Pls3*-deficient mice, when we measured the circulating levels of both, Sfrp4 and Wnt16 (Fig. 4F).

During the course of our studies we identified a 22 years old man

Fig. 5. Skeletal analysis of a patient with *PLS3*-associated osteoporosis in comparison to *Pls3*-deficient mice. (A) Segregation analysis and pedigree of the family. The arrow indicates the index patient. (B) BMD values (Z-score) of the patient at the spine and hip as determined by DXA. (C) Structural parameters of the patient's distal radius as determined by HR-pQCT compared to age- and sex-matched reference data [22]. (D) μ-CT and histological section of a iliac crest biopsy from the patient with *PLS3*-associated osteoporosis obtained at the age of 18 years. Goldner stain. Scale bar = 1 mm. (E) Structural parameters of the iliac crest biopsy in comparison to age- and gender-matched reference ranges (grey hatched lines) [23]. (F) qBEI micrographs of cortical and trabecular bone of the patient's iliac crest biopsy. Scale bar = 200 μm. (G) qBEI based analysis of the calcium mineral distribution in the transiliac biopsy in comparison to skeletal healthy age- and gender-matched controls [24]. (H) qBEI images of cortical bone from tibia of 12 weeks old $Pls3^{+/0}$ and $Pls3^{-/0}$ mice. (I) qBEI based analysis of the calcium mineral distribution in the femoral cortical bone of 12 weeks old male $Pls3^{+/0}$ and $Pls3^{-/0}$ mice. (J) Mean Ca^{2+} mineral content in the femoral cortical bone of 12 weeks old male $Pls3^{+/0}$ and $Pls3^{-/0}$ mice as determined by qBEI. (K) Endocortical osteoid thickness of the femoral cortical bone of 12 weeks old male $Pls3^{+/0}$ and $Pls3^{-/0}$ mice. Data were analyzed by Student's *t*-test. n ≥ 5 mice per group. *p < 0.05 vs. controls.

with a hemizygous intronic mutation (1512-1G > T) of *PLS3*. As evidenced by Mutation Taster [36] this mutation is likely pathogenic by interference with a splice acceptor site. While the mutation was also detected in the mother, we did not detect it in the index patient's brother. Of note, the uncle of the patient had been diagnosed with osteogenesis imperfecta, yet we did not have access to blood samples. Whereas DXA Z-scores were within the reference range for the carrier mother and the unaffected brother (Fig.5A), the index patient displayed severe osteoporosis based on DXA Z-scores at the lumbar spine and hip (Fig. 5B). We additionally applied high-resolution peripheral quantitative computed tomography (HR-pQCT) to determine trabecular and cortical bone parameters in the distal radius. Here we observed, when compared to age- and gender-matched reference ranges, that the trabecular bone volume was remarkably reduced in the patient, and that the cortical thinning was even more pronounced (Fig. 5C). Similar findings were obtained by histomorphometric analysis of a transiliac bone biopsy, yet there was no pathologic enrichment of osteoid (Fig. 5D and E). To analyze the calcium distribution within the mineralized bone matrix we further applied quantitative backscattered electron imaging (qBEI), thereby revealing a shift towards a lower mineral content, in line with previously published data (Fig. 5F and G). Based on this finding we used the same methods to analyze the cortical bone of *Pls3*-deficient mice for potential mineralization defects (Fig. 5H). Here we did, however, not observe a difference towards wildtype littermates in terms of mineral content (Fig. 5I and J) or osteoid thickness (Fig. 5K).

Despite the fact that the *Pls3*-deficient mice did not fully recapitulate the skeletal defects observed in patients with inactivating *PLS3* mutation, we utilized them to address the question, if *Pls3*-deficiency would impair the response to osteoanabolic PTH injection. In fact, the above described patient was treated by a combination of teriparatide and denosumab in the first year due to the severe bone phenotype. Thereafter, teriparatide was omitted, i.e. the subsequent treatment was only performed by denosumab. Of note, the evaluation of trabecular and cortical bone mass using HR-pQCT revealed a stronger positive influence in the first year, suggesting that teriparatide is most beneficial for the treatment of *PLS3*-dependent osteoporosis (Fig. 6A). This led us to investigate the response of *Pls3*-deficient mice to an intermittent PTH treatment. After two weeks of daily PTH injection the *Pls3*-deficient mice displayed increased osteoblastogenesis (Fig. 6B) and bone formation rate (Fig. 6C) in the trabecular compartment with an extent that was comparable to wildtype littermates. Similar responses were observed for periosteal and endocortical bone formation rates, although the variability of both parameters was too high to reach statistical significance compared to untreated *Pls3*-deficient controls (Fig. 6D). Importantly however, despite the short treatment duration that was designed to detect the cellular response, the cortical thickness was significantly increased in both, wildtype and *Pls3*-deficient mice (Fig. 6E), thereby demonstrating that *Pls3*-deficiency does not interfere with osteoanabolic PTH treatment.

4. Discussion

PLS3 contains two actin-binding domains that allow the interconnection of F-actin fibers to facilitate shaping of specific cytoskeletal configurations [1]. *Pls3* expression is not restricted to skeletal types, which was also evident in our own qRT-PCR expression analysis using RNA from different tissues and cultured bone remodeling cells. Based on this ubiquitous expression pattern, but also given the importance of cytoskeletal dynamics for many different cell types, it is surprising that mutations of *PLS3* only impact specific organs. More specifically, *PLS3* is an established modulator of disease severity in spinal muscular atrophy, although the primary disease-causing mutation is within the *SMN1* gene [37]. The only disorder where mutations in *PLS3* were identified as causative is X-linked osteoporosis. While the clinical characterization of the respective patients is fairly comprehensive [2–4,6–8], the cellular and molecular mechanism explaining the impact of PLS3 on the skeleton are poorly understood.

A first study regarding the skeletal phenotype of a *Pls3*-deficient mouse model was recently published [11]. Here it was found that 12 weeks old male *Pls3*-deficient mice display decreased cortical thickness, whereas 12 weeks old female *Pls3*-deficient mice also displayed a moderately reduced trabecular bone mass. As we obtained the same results by analyzing female mice, our data are fully confirming these previous findings. This also applies to three-point bending assays, where femoral bones from 12 weeks old male *Pls3*-deficient mice displayed reduced biomechanical stability. Since the previous study, which also included a mouse model with *Pls3*-overexpression, demonstrated a function of PLS3 as a negative regulator of osteoclastogenesis, it is further important to state that we observed increased cortical porosity in 6 to 24 weeks old *Pls3*-deficient mice, as well as increased calvarial porosity in 24 weeks old *Pls3*-deficient mice.

To expand the knowledge on the putative function of PLS3 in bone metabolism, we extended the analysis of *Pls3*-deficient mice by applying histomorphometry on undecalcified bone sections and by analyzing different age groups. Here we found a remarkable reduction of cortical thickness compared to wildtype littermates at all ages analyzed. Importantly however, the relative cortical thickness gain, when compared to the status of 3 weeks old mice, was identical between wildtype and *Pls3*-deficient littermates. These data clearly demonstrate that the major defect of *Pls3*-deficient mice is a reduced cortical bone acquisition establishing before weaning. This also explains, why there was no histomorphometric difference observed, when the mice were analyzed at 12 weeks of age. Likewise, we did not detect significant differences in the serum concentration of biomarkers for bone formation and resorption or in the ratio of circulating Rankl and Opg between 12 weeks old wildtype and *Pls3*-deficient mice.

Since the reduced cortical bone acquisition in *Pls3*-deficient mice is most likely explained by an impairment of osteoblast lineage cells, we additionally isolated primary osteoblasts. Here we found that *Pls3*-deficient cells displayed a moderate, yet significant impairment of mineralized matrix formation. Although it is still possible that the lack of Pls3 is compensated by the other family members, we did not observe a transcriptional activation of *Pls1* and *Pls2* in *Pls3*-deficient primary osteoblasts. Moreover, the expression of most osteoblast marker genes was not different between wildtype and *Pls3*-deficient osteoblasts, with the notable exceptions of *Bglap, Sfrp4*, and *Wnt16*, all displaying reduced expression in the absence of *Pls3*. Especially Sfrp4, a secreted Wnt-signaling antagonist, could be relevant in the context of the observed skeletal phenotype in *Pls3*-deficient mice, since Sfrp4 inactivation specifically causes cortical thinning, in mice and humans [28,34].

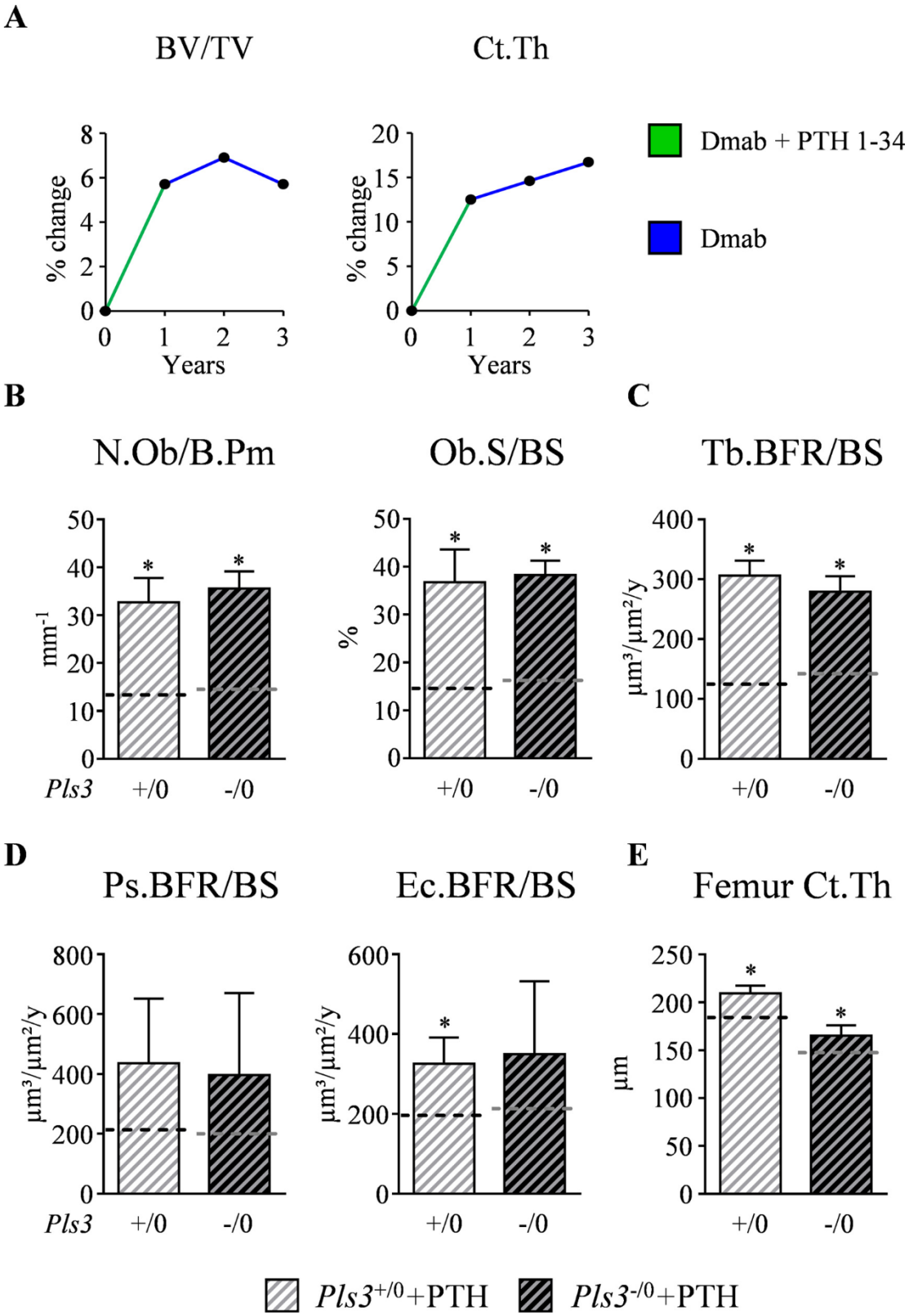

Fig. 6. Osteoanabolic treatment response of a patient with *PLS3*-associated osteoporosis and *Pls3*-deficient mice. (A) HR-pQCT based evaluation of changes of the microarchitectural composition of the distal radius of the patient with *PLS3*-associated osteoporosis during treatment. All values are relative to the status at the beginning of the treatment. The patient received combined denosumab (Dmab) and teriparatide (PTH 1–34) during the first year of treatment and Dmab only from the second year. (B) Osteoblast number and surface determined in the trabecular bone of vertebral bodies of 12 weeks old $Pls3^{+/0}$ and $Pls3^{-/0}$ mice after 2 weeks of osteoanabolic treatment with daily injections of rhPTH 1-34. The dashed lines indicate the mean value of untreated controls of the respective genotypes. (C) Trabecular bone formation rate in the vertebral bodies of the same mice as described in subpanel B. (D) Bone formation rate of the cortical bone in the mid diaphyseal region of femora from the same mice as described in subpanel B. (E) Cortical thickness of mid diaphyseal region of femora from the same mice as described in subpanel B as determined by µCT. Data were analyzed by Student's *t*-test. n = 5 mice per group. *p < 0.05 vs. untreated controls of the respective genotype.

Whether the reduced expression of *Sfrp4* in *Pls3*-deficient osteoblasts is linked to the development of the cortical bone phenotype of *Pls3*-deficient mice remains to be established. At present we can only state that we did not observe reduced serum concentrations of Sfrp4 in *Pls3*-deficient mice. Moreover, since Sfrp4-deficiency also reduces calvarial thickness, which was not the case in *Pls3*-deficient mice, it is unlikely, that the primary function of PLS3 in osteoblasts is to control specifically Sfrp4 production. The same applies for the relevance of reduced *Wnt16* expression in primary *Pls3*-deficient osteoblasts. Whereas the *WNT16* locus, based on genome-wide association studies, was found associated with cortical thickness and nonvertebral fractures [38], *Wnt16*-deficient mice were found to specifically display a cortical bone phenotype with increased porosity [30]. This phenotype is primarily explained by the lack of the inhibitory action of Wnt16 on osteoclastogenesis. Therefore, decreased *Wnt16* expression in *Pls3*-deficient osteoblasts may be relevant to explain the cortical and calvarial porosity in *Pls3*-deficient mice, yet again, the circulating levels of Wnt16 were not different compared to wildtype littermates.

One major limitation of the *Pls3*-deficient mouse model is the phenotypic discrepancy towards X-linked osteoporosis in humans. This does not only apply to the respective literature reports on patients with inactivating *PLS3* mutation, but also to the patient described in the present manuscript. Here we observed a marked reduction in both, cortical and trabecular bone mass, as well as reduced calcium content within the mineralized bone matrix. At present we can only speculate about the cause for the apparent inconsistency between mouse and human data, especially since there are only few examples for other deficiency models that do not fully recapitulate pathologies observed in the respective patients [39–41]. The most likely explanation is that *Pls3*-deficient mice, in contrast to the majority of patients with X-linked osteoporosis, lack the entire *Pls3* gene, which excludes a potential influence of the mutated protein. To circumvent this problem, it might be required to generate a knockin model for X-linked osteoporosis in the future. Additionally, external factors such as nutrition or environmental conditions might influence the skeletal characteristics as well. On the other hand, since we did observe, similar to the patients, an impact of *Pls3*-deficiency on cortical bone mass, we decided to utilize this model in order to analyze its response to osteoanabolic PTH treatment. Here we could clearly detect that *Pls3*-deficient mice responded to the same extent as their littermate controls, which fully supports the results of a previously published pilot study, where three patients with *PLS3* mutations were successfully treated with teriparatide [9].

A second limitation of our study is that we were unable to provide a plausible molecular mechanism explaining the specific cortical bone phenotype of *Pls3*-deficient mice. This is mostly attributed to the lack of an obvious cellular defect of *Pls3*-deficient primary osteoblasts. Here it is also important to state that we did not observe major abnormalities of *Pls3*-deficient cells in terms of morphology, nor in adhesion or migration assays. It might be worthwhile to perform more thorough analyses in future experiments to analyze the possibility that Pls3-deficiency impacts protein secretion by interfering with the formation of an actomyosin II ring [42–44], but such studies are beyond the scope of the present manuscript. However, since the relevance of such cell culture experiments in the context of a site-specific skeletal phenotype is generally debatable, we truly believe that the disrupted osteoblast surfaces in the periosteal bone regions with 4 mm distance from the growth plate, are probably more informative. In fact, one could speculate that the alignment of osteoblasts into one layer of cells at the cortical bone surfaces requires specific cytoskeletal rearrangements, which could be disturbed in *Pls3*-deficient mice. Moreover, since the bone-forming units are typically shorter in the trabecular compartment of murine bones, the specific impact of *Pls3*-deficiency might be less relevant at these sites.

Regardless of these limitations, we truly believe that it was important to study the skeletal phenotype of *Pls3*-deficient mice, at different ages, on the basis of undecalcified histology and bone-specific histomorphometry, since the relevance of PLS3 for human bone mass acquisition is undoubted. Our findings extend the previous knowledge regarding the skeletal phenotype of *Pls3*-deficient mice, which do not only display increased osteoclastogenesis, but also a unique cortical bone phenotype establishing at an early postnatal stage.

Funding

Grant supporters: This project has received funding from the Deutsche Forschungsgemeinschaft (AM 103/30-1,SCHI 504/12-1), the European Community's Seventh Framework Programme under grant agreement no. 602,300 (SYBIL), and the German Federal Ministry of Education and Research (BMBF)within the project "Detection and Individualized Management of Early Onset Osteoporosis (DIMEOS)".

Declaration of Competing Interest

All authors state that they have no conflict of interest.

Acknowledgements

We would like to thank the UKE research animal facility for their services. Moreover we would like to express our gratitude to Lana Rosenthal, Olga Winter, Mona Neven, Stephanie Peters, Elke Leicht and Annica Pröhl, for their technical assistance and Tina Wallaschkowski and Tonia Bargmann for their assistance during their internship.

Authors' roles: Study design: TAY, MA, TS. Study conduct: TAY, HS, TR, SW, AVF, UK, RO. Data interpretation: TAY, TR, SW, UK, RO, MA, TS. Drafting manuscript: TAY, TR and TS. Revising manuscript: all authors. Approving manuscript for publication: all authors.

Appendix A. Supplementary data

Supplementary material related to this article can be found, in the online version, at doi:https://doi.org/10.1016/j.bone.2019.115062.

References

[1] V. Delanote, J. Vandekerckhove, J. Gettemans, Plastins: versatile modulators of actin organization in (patho)physiological cellular processes, Acta Pharmacol. Sin. 26 (7) (2005) 769–779.

[2] F.S. van Dijk, M.C. Zillikens, D. Micha, M. Riessland, C.L. Marcelis, C.E. de Die-Smulders, J. Milbradt, A.A. Franken, A.J. Harsevoort, K.D. Lichtenbelt, H.E. Pruijs, M.E. Rubio-Gozalbo, R. Zwertbroek, Y. Moutaouakil, J. Egthuijsen, M. Hammerschmidt, R. Bijman, C.M. Semeins, A.D. Bakker, V. Everts, J. Klein-Nulend, N. Campos-Obando, A. Hofman, G.J. te Meerman, A.J. Verkerk, A.G. Uitterlinden, A. Maugeri, E.A. Sistermans, Q. Waisfisz, H. Meijers-Heijboer, B. Wirth, M.E. Simon, G. Pals, PLS3 mutations in X-linked osteoporosis with fractures, N. Engl. J. Med. 369 (16) (2013) 1529–1536.

[3] S. Fahiminiya, J. Majewski, H. Al-Jallad, P. Moffatt, J. Mort, F.H. Glorieux, P. Roschger, K. Klaushofer, F. Rauch, Osteoporosis caused by mutations in PLS3: clinical and bone tissue characteristics, J. Bone Miner. Res. 29 (8) (2014) 1805–1814.

[4] C.M. Laine, M. Wessman, S. Toiviainen-Salo, M.A. Kaunisto, M.K. Mayranpaa, T. Laine, M. Pekkinen, H. Kroger, V.V. Valimaki, M.J. Valimaki, A.E. Lehesjoki, O. Makitie, A novel splice mutation in PLS3 causes X-linked early onset low-turnover osteoporosis, J. Bone Miner. Res. 30 (3) (2015) 510–518.

[5] K. Wesseling-Perry, R.E. Makitie, V.V. Valimaki, T. Laine, C.M. Laine, M.J. Valimaki, R.C. Pereira, O. Makitie, Osteocyte protein expression is altered in low-turnover osteoporosis caused by mutations in WNT1 and PLS3, J. Clin. Endocrinol. Metab. 102 (7) (2017) 2340–2348.

[6] A.J. Kämpe, A. Costantini, R.E. Makitie, N. Jantti, H. Valta, M. Mayranpaa, H. Kroger, M. Pekkinen, F. Taylan, H. Jiao, O. Makitie, PLS3 sequencing in childhood-onset primary osteoporosis identifies two novel disease-causing variants, Osteoporos. Int. 28 (10) (2017) 3023–3032.

[7] A.J. Kämpe, A. Costantini, Y. Levy-Shraga, L. Zeitlin, P. Roschger, F. Taylan, A. Lindstrand, E.P. Paschalis, S. Gamsjaeger, A. Raas-Rothschild, M. Hovel, H. Jiao, K. Klaushofer, C. Grasemann, O. Makitie, PLS3 deletions lead to severe spinal osteoporosis and disturbed bone matrix mineralization, J. Bone Miner. Res. 32 (12) (2017) 2394–2404.

[8] A. Costantini, P. Krallis, A. Kampe, E.M. Karavitakis, F. Taylan, O. Makitie, A. Doulgeraki, A novel frameshift deletion in PLS3 causing severe primary osteoporosis, J. Hum. Genet. 63 (8) (2018) 923–926.

[9] V.V. Välimäki, O. Makitie, R. Pereira, C. Laine, K. Wesseling-Perry, J. Maatta,

M. Kirjavainen, H. Viljakainen, M.J. Valimaki, Teriparatide treatment in patients with WNT1 or PLS3 mutation-related early-onset osteoporosis: a pilot study, J. Clin. Endocrinol. Metab. 102 (2) (2017) 535–544.
[10] H. Kamioka, Y. Sugawara, T. Honjo, T. Yamashiro, T. Takano-Yamamoto, Terminal differentiation of osteoblasts to osteocytes is accompanied by dramatic changes in the distribution of actin-binding proteins, J. Bone Miner. Res. 19 (3) (2004) 471–478.
[11] J. Neugebauer, J. Heilig, S. Hosseinibarkooie, B.C. Ross, N. Mendoza-Ferreira, F. Nolte, M. Peters, I. Holker, K. Hupperich, T. Tschanz, V. Grysko, F. Zaucke, A. Niehoff, B. Wirth, Plastin 3 influences bone homeostasis through regulation of osteoclast activity, Hum. Mol. Genet. 27 (24) (2018) 4249–4262.
[12] J. Keller, P. Catala-Lehnen, A.K. Huebner, A. Jeschke, T. Heckt, A. Lueth, M. Krause, T. Koehne, J. Albers, J. Schulze, S. Schilling, M. Haberland, H. Denninger, M. Neven, I. Hermans-Borgmeyer, T. Streichert, S. Breer, F. Barvencik, B. Levkau, B. Rathkolb, E. Wolf, J. Calzada-Wack, F. Neff, V. Gailus-Durner, H. Fuchs, M.H. de Angelis, S. Klutmann, E. Tsourdi, L.C. Hofbauer, B. Kleuser, J. Chun, T. Schinke, M. Amling, Calcitonin controls bone formation by inhibiting the release of sphingosine 1-phosphate from osteoclasts, Nat. Commun. 5 (2014) 5215.
[13] J. Albers, J. Keller, A. Baranowsky, F.T. Beil, P. Catala-Lehnen, J. Schulze, M. Amling, T. Schinke, Canonical Wnt signaling inhibits osteoclastogenesis independent of osteoprotegerin, J. Cell Biol. 200 (4) (2013) 537–549.
[14] D.W. Dempster, J.E. Compston, M.K. Drezner, F.H. Glorieux, J.A. Kanis, H. Malluche, P.J. Meunier, S.M. Ott, R.R. Recker, A.M. Parfitt, Standardized nomenclature, symbols, and units for bone histomorphometry: a 2012 update of the report of the ASBMR Histomorphometry Nomenclature Committee, J. Bone Miner. Res. 28 (1) (2013) 2–17.
[15] P. Milovanovic, E.A. Zimmermann, C. Riedel, A. vom Scheidt, L. Herzog, M. Krause, D. Djonic, M. Djuric, K. Puschel, M. Amling, R.O. Ritchie, B. Busse, Multi-level characterization of human femoral cortices and their underlying osteocyte network reveal trends in quality of young, aged, osteoporotic and antiresorptive-treated bone, Biomaterials 45 (2015) 46–55.
[16] P. Roschger, P. Fratzl, J. Eschberger, K. Klaushofer, Validation of quantitative backscattered electron imaging for the measurement of mineral density distribution in human bone biopsies, Bone 23 (4) (1998) 319–326.
[17] P. Roschger, E.P. Paschalis, P. Fratzl, K. Klaushofer, Bone mineralization density distribution in health and disease, Bone 42 (3) (2008) 456–466.
[18] T.A. Yorgan, S. Peters, A. Jeschke, P. Benisch, F. Jakob, M. Amling, T. Schinke, The anti-osteoanabolic function of sclerostin is blunted in mice carrying a high bone mass mutation of Lrp5, J. Bone Miner. Res. 30 (7) (2015) 1175–1183.
[19] M.L. Bouxsein, S.K. Boyd, B.A. Christiansen, R.E. Guldberg, K.J. Jepsen, R. Muller, Guidelines for assessment of bone microstructure in rodents using micro-computed tomography, J. Bone Miner. Res. 25 (7) (2010) 1468–1486.
[20] J. Luther, T.A. Yorgan, T. Rolvien, L. Ulsamer, T. Koehne, N. Liao, D. Keller, N. Vollersen, S. Teufel, M. Neven, S. Peters, M. Schweizer, A. Trumpp, S. Rosigkeit, E. Bockamp, S. Mundlos, U. Kornak, R. Oheim, M. Amling, T. Schinke, J.P. David, Wnt1 is an Lrp5-independent bone-anabolic Wnt ligand, Sci. Transl. Med. 10 (466) (2018).
[21] J. Schulze, T. Bickert, F.T. Beil, M.M. Zaiss, J. Albers, K. Wintges, T. Streichert, K. Klaetschke, J. Keller, T.N. Hissnauer, A.S. Spiro, A. Gessner, G. Schett, M. Amling, A.N. McKenzie, A.K. Horst, T. Schinke, Interleukin-33 is expressed in differentiated osteoblasts and blocks osteoclast formation from bone marrow precursor cells, J. Bone Miner. Res. 26 (4) (2011) 704–717.
[22] H.M. Macdonald, K.K. Nishiyama, J. Kang, D.A. Hanley, S.K. Boyd, Age-related patterns of trabecular and cortical bone loss differ between sexes and skeletal sites: a population-based HR-pQCT study, J. Bone Miner. Res. 26 (1) (2011) 50–62.
[23] F.H. Glorieux, R. Travers, A. Taylor, J.R. Bowen, F. Rauch, M. Norman, A.M. Parfitt, Normative data for iliac bone histomorphometry in growing children, Bone 26 (2) (2000) 103–109.
[24] T. Rolvien, T. Koehne, U. Kornak, W. Lehmann, M. Amling, T. Schinke, R. Oheim, A novel ANO5 mutation causing gnathodiaphyseal dysplasia with high bone turnover osteosclerosis, J. Bone Miner. Res. 32 (2) (2017) 277–284.
[25] T. Schmidt, D. Schwinge, T. Rolvien, A. Jeschke, C. Schmidt, M. Neven, S. Butscheidt, M. Kriz, L. Kunzmann, H. Mussawy, J. Hubert, T. Hawellek, W. Ruther, R. Oheim, F. Barvencik, A.W. Lohse, C. Schramm, T. Schinke, M. Amling, Th17 cell frequency is associated with low bone mass in primary sclerosing cholangitis, J. Hepatol. (2019).
[26] F. Faul, E. Erdfelder, A.G. Lang, A. Buchner, G*Power 3: a flexible statistical power analysis program for the social, behavioral, and biomedical sciences, Behav. Res. Methods 39 (2) (2007) 175–191.
[27] H. Rios, S.V. Koushik, H. Wang, J. Wang, H.M. Zhou, A. Lindsley, R. Rogers, Z. Chen, M. Maeda, A. Kruzynska-Frejtag, J.Q. Feng, S.J. Conway, Periostin null mice exhibit dwarfism, incisor enamel defects, and an early-onset periodontal disease-like phenotype, Mol. Cell. Biol. 25 (24) (2005) 11131–11144.
[28] R. Haraguchi, R. Kitazawa, K. Mori, R. Tachibana, H. Kiyonari, Y. Imai, T. Abe, S. Kitazawa, sFRP4-dependent Wnt signal modulation is critical for bone remodeling during postnatal development and age-related bone loss, Sci. Rep. 6 (2016) 25198.
[29] A. Jeschke, P. Catala-Lehnen, S. Sieber, T. Bickert, M. Schweizer, T. Koehne, K. Wintges, R.P. Marshall, A. Mautner, L. Duchstein, B. Otto, A.K. Horst, M. Amling, H.J. Kreienkamp, T. Schinke, Sharpin controls osteogenic differentiation of mesenchymal bone marrow cells, J. Immunol. 195 (8) (2015) 3675–3684.
[30] S. Moverare-Skrtic, P. Henning, X. Liu, K. Nagano, H. Saito, A.E. Borjesson, K. Sjogren, S.H. Windahl, H. Farman, B. Kindlund, C. Engdahl, A. Koskela, F.P. Zhang, E.E. Eriksson, F. Zaman, A. Hammarstedt, H. Isaksson, M. Bally, A. Kassem, C. Lindholm, O. Sandberg, P. Aspenberg, L. Savendahl, J.Q. Feng, J. Tuckermann, J. Tuukkanen, M. Poutanen, R. Baron, U.H. Lerner, F. Gori, C. Ohlsson, Osteoblast-derived WNT16 represses osteoclastogenesis and prevents cortical bone fragility fractures, Nat. Med. 20 (11) (2014) 1279–1288.
[31] J.E. Wergedal, C. Kesavan, R. Brommage, S. Das, S. Mohan, Role of WNT16 in the regulation of periosteal bone formation in female mice, Endocrinology 156 (3) (2015) 1023–1032.
[32] R. Brommage, C. Ohlsson, Translational studies provide insights for the etiology and treatment of cortical bone osteoporosis, Best Pract. Res. Clin. Endocrinol. Metab. 32 (3) (2018) 329–340.
[33] C. Galada, H. Shah, A. Shukla, K.M. Girisha, A novel sequence variant in SFRP4 causing Pyle disease, J. Hum. Genet. 62 (5) (2017) 575–576.
[34] P.O.S. Kiper, H. Saito, F. Gori, S. Unger, E. Hesse, K. Yamana, R. Kiviranta, N. Solban, J. Liu, R. Brommage, K. Boduroglu, L. Bonafe, B. Campos-Xavier, E. Dikoglu, R. Eastell, F. Gossiel, K. Harshman, G. Nishimura, K.M. Girisha, B.J. Stevenson, H. Takita, C. Rivolta, A. Superti-Furga, R. Baron, Cortical-bone fragility–Insights from sFRP4 deficiency in Pyle's disease, N. Engl. J. Med. 374 (26) (2016) 2553–2562.
[35] N. Chatron, G. Lesca, A. Labalme, P.A. Rollat-Farnier, P. Monin, E. Pichot, P. Edery, D. Sanlaville, M. Rossi, A novel homozygous truncating mutation of the SFRP4 gene in Pyle's disease, Clin. Genet. 92 (1) (2017) 112–114.
[36] J.M. Schwarz, D.N. Cooper, M. Schuelke, D. Seelow, MutationTaster2: mutation prediction for the deep-sequencing age, Nat. Methods 11 (4) (2014) 361–362.
[37] G.E. Oprea, S. Krober, M.L. McWhorter, W. Rossoll, S. Muller, M. Krawczak, G.J. Bassell, C.E. Beattie, B. Wirth, Plastin 3 is a protective modifier of autosomal recessive spinal muscular atrophy, Science 320 (5875) (2008) 524–527.
[38] H.F. Zheng, J.H. Tobias, E. Duncan, D.M. Evans, J. Eriksson, L. Paternoster, L.M. Yerges-Armstrong, T. Lehtimaki, U. Bergstrom, M. Kahonen, P.J. Leo, O. Raitakari, M. Laaksonen, G.C. Nicholson, J. Viikari, M. Ladouceur, L.P. Lyytikainen, C. Medina-Gomez, F. Rivadeneira, R.L. Prince, H. Sievanen, W.D. Leslie, D. Mellstrom, J.A. Eisman, S. Moverare-Skrtic, D. Goltzman, D.A. Hanley, G. Jones, B. St Pourcain, Y. Xiao, N.J. Timpson, G.D. Smith, I.R. Reid, S.M. Ring, P.N. Sambrook, M. Karlsson, E.M. Dennison, J.P. Kemp, P. Danoy, A. Sayers, S.G. Wilson, M. Nethander, E. McCloskey, L. Vandenput, R. Eastell, J. Liu, T. Spector, B.D. Mitchell, E.A. Streeten, R. Brommage, U. Pettersson-Kymmer, M.A. Brown, C. Ohlsson, J.B. Richards, M. Lorentzon, WNT16 influences bone mineral density, cortical bone thickness, bone strength, and osteoporotic fracture risk, PLoS Genet. 8 (7) (2012) e1002745.
[39] A. Patoine, A. Husseini, B. Kasaai, M.H. Gaumond, P. Moffatt, The osteogenic cell surface marker BRIL/IFITM5 is dispensable for bone development and homeostasis in mice, PLoS One 12 (9) (2017) e0184568.
[40] K.G. Waymire, J.D. Mahuren, J.M. Jaje, T.R. Guilarte, S.P. Coburn, G.R. MacGregor, Mice lacking tissue non-specific alkaline phosphatase die from seizures due to defective metabolism of vitamin B-6, Nat. Genet. 11 (1) (1995) 45–51.
[41] R. Brommage, C. Ohlsson, High fidelity of mouse models mimicking human genetic skeletal disorders resulting from mutations in 316 genes (Skeletal dysplasia society 2015 nosology update), J. Bone Miner. Res. 33 (S1) (2018) S226.
[42] E. Dor-On, S. Raviv, Y. Cohen, O. Adir, K. Padmanabhan, C. Luxenburg, T-plastin is essential for basement membrane assembly and epidermal morphogenesis, Sci. Signal. 10 (481) (2017).
[43] T.D. Nightingale, I.J. White, E.L. Doyle, M. Turmaine, K.J. Harrison-Lavoie, K.F. Webb, L.P. Cramer, D.F. Cutler, Actomyosin II contractility expels von Willebrand factor from Weibel-Palade bodies during exocytosis, J. Cell Biol. 194 (4) (2011) 613–629.
[44] C. Thouverey, A. Malinowska, M. Balcerzak, A. Strzelecka-Kiliszek, R. Buchet, M. Dadlez, S. Pikula, Proteomic characterization of biogenesis and functions of matrix vesicles released from mineralizing human osteoblast-like cells, J. Proteomics 74 (7) (2011) 1123–1134.